The effect of Nb doping on the performance and stability of TiO_x devices

2013 J. Phys. D: Appl. Phys. 46 295102

(http://iopscience.iop.org/0022-3727/46/29/295102)

J. Phys. D: Appl. Phys. **46** (2013) 295102 (5pp) doi:10.1088/0022-3727/46/29/295102

The effect of Nb doping on the performance and stability of TiO_x devices

Kyung-Chul Ok[1,4], Yoseb Park[1,4], Kwun-Bum Chung[2,3] and Jin-Seong Park[1,3]

[1] Division of Materials Science and Engineering, Hanyang University, 222 Wangsimni-ro, Seongdong-gu, Seoul 133–791, Republic of Korea
[2] Department of Physcis, Dankook University, 119 Dandae-ro, Dongnam-gu, Cheonan 330–714, Republic of Korea

E-mail: jsparklime@hanyang.ac.kr (J-S Park), kbchung@dankook.ac.kr (K-B Chung), kchul2926@naver.com (K-C Ok) and jozeph.park@gmail.com (Y Park)

Received 10 March 2013, in final form 16 May 2013
Published 27 June 2013
Online at stacks.iop.org/JPhysD/46/295102

Abstract
The effect of niobium (Nb) doping on the performance and stability of TiO_x-based thin-film transistors (TFTs) was studied. While sputtered TiO_x has an initial amorphous phase and begins to crystallize to anatase at an annealing temperature of 450 °C, Nb-doped TiO_x preserves the amorphous structure up to annealing temperatures as high as 550 °C. TFT devices fabricated using Nb-doped TiO_x as the active layer exhibit higher field-effect mobility and better stability upon negative and positive bias stress compared to pure TiO_x devices. X-ray photoelectron spectroscopy analyses indicate that Nb doping induces higher levels of oxygen deficiency and a considerable amount of defect states near the valence band, which cannot account for the higher device stability. It is thus suggested that the grain boundaries in crystalline TiO_xTiO_x may act as the major charge traps, which induce larger shifts in threshold voltage (V_{th}) upon bias stress.

(Some figures may appear in colour only in the online journal)

1. Introduction

Amorphous oxide semiconductors (AOSs) have recently drawn a lot of attention for potential use in flat panel displays (FPDs), owing to the possibility to deposit them easily over large areas using conventional sputtering techniques at room temperature. Indium and zinc based oxides such as indium zinc oxide (IZO) or indium gallium zinc oxide (IGZO) have been the main components being studied since the report on amorphous IGZO (a-IGZO) thin-film transistors (TFTs) by Hosono *et al* [1, 2].

Alternative materials have also been investigated constantly in order to find substances that are cost effective compared to relatively expensive indium, and in this regard titanium oxide (TiO_x) is a good candidate material that exhibits electrical properties either as a transparent conducting oxide (TCO) or a semiconductor [3–5].

Several former studies on the behaviour of TiO_x with respect to its structural characteristics are available in the literature, and in particular the effects of doping this material with elements such as niobium (Nb) [6], vanadium (V) [7] and cerium (Ce) [8] are reported to result in high electrical conductivity.

This work consists of a comparison of two different types of TFT devices, each using pure TiO_x and Nb-doped TiO_x (TNO hereafter) as the active material. The structure and electrical properties are evaluated, and the device stability with respect to positive and negative bias stress is also examined. It is found that the addition of Nb promotes the preservation of an amorphous phase up to high annealing temperatures, and results in devices with higher performance and stability than those fabricated using pure TiO_x.

2. Experimental details

In order to study the individual film properties, TiO_x and TNO films were deposited on heavily doped p^{++}-Si wafers with thermally grown SiO_2 (100 nm) using radio frequency (RF) magnetron sputtering. Oxygen-deficient ($x < 2$) 3 inch targets of TiO_x and TNO were used, the composition of the TNO target being approximately 10 wt% NbO_x in TiO_x matrix. The RF power and process pressure were kept at 75 W and 10 mTorr, respectively. Only Ar gas was used with a flow rate of 50 sccm, and the final thickness of the films was 30 nm. The films were thermally treated in air for 1 h at different temperatures up to 550 °C, and the structural properties were observed using x-ray diffraction (XRD) and transmission electron microscopy (TEM). Rutherford backscattering spectroscopy (RBS) analyses were done in

[3] Authors to whom any correspondence should be addressed.
[4] Contributed to this work equally.

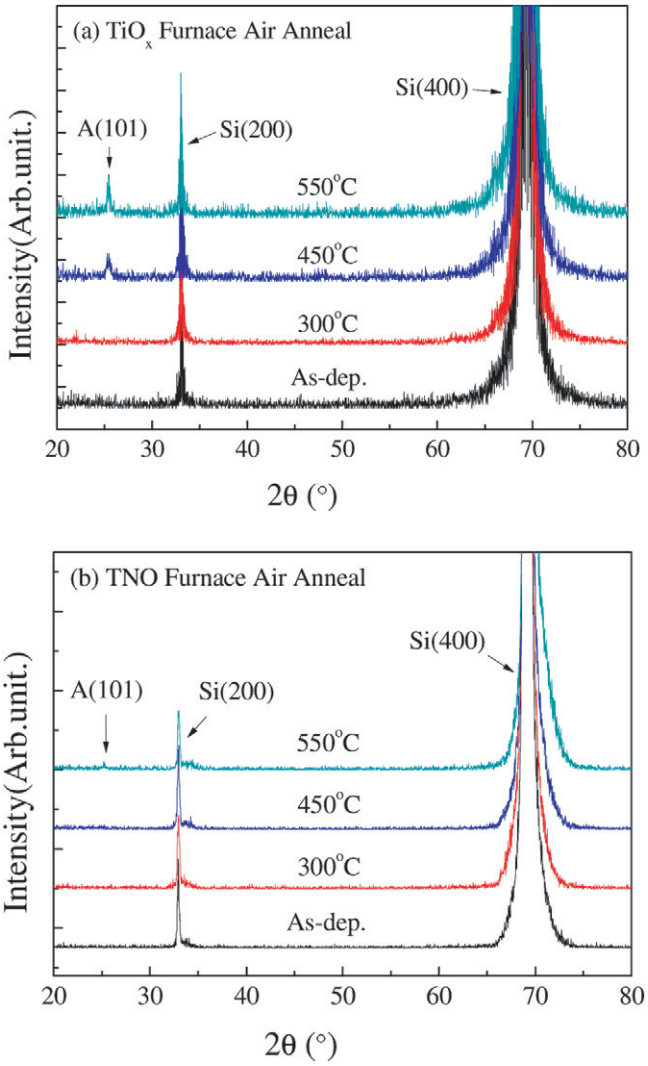

Figure 1. XRD patterns for the (*a*) TiO_x and (*b*) TNO films, in the as-deposited state and after heat treatment in air at different temperatures.

order to study the actual composition of the deposited films. The electronic properties were also studied by x-ray photoelectron spectroscopy (XPS). The optical band gap was extracted by spectroscopic ellipsometry (SE).

TFT devices were fabricated by depositing the active layers through shadow masks on identical substrates, again with a final thickness of 30 nm. Prior to depositing the source/drain (S/D) electrodes, thermal treatments were performed in air for 1 h at 450 °C. Then, 100 nm thick indium tin oxide (ITO) electrodes were deposited through shadow masks to form the S/D electrodes. Devices with width (W) of 1000 μm and length (L) of 150 μm, were studied in this work.

3. Results and discussion

Figures 1(*a*) and (*b*) show the XRD patterns for the TiO_x and TNO films, respectively. The as-deposited films are initially amorphous, and a crystalline anatase phase develops at 450 °C in TiO_x. The results are consistent with previous reports [9–11], which indicated the appearance of anatase phase at

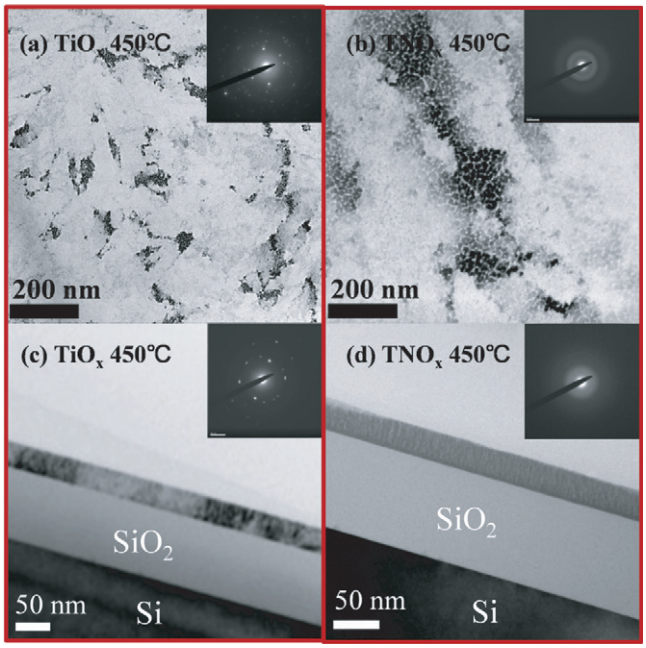

Figure 2. Plan-view TEM images of the (*a*) TiO_x film and (*b*) TNO film annealed at 450 °C. Cross-sectional TEM images of the (*c*) TiO_x film and (*d*) TNO film annealed at 450 °C.

annealing temperatures between 300 to 450 °C, depending on the deposition and/or annealing conditions. A small fraction of anatase phase is observed in TNO when annealed at 550 °C.

TEM images of the TiO_x and TNO films annealed at 450 °C are illustrated in figure 2, confirming the presence of crystallites in TiO_x, and an amorphous film in the case of TNO.

RBS analyses indicate that the Ti : O ratio in the TiO_x film is approximately 1 : 1.7, which reflects that the film is slightly oxygen deficient, in comparison with a perfect stoichiometry of 1 : 2. The Nb : Ti ratio in the TNO film is approximately 18 : 82, thus the film slightly contains high Nb dopant (about 4.7 at%) in sputtered films.

XPS studies were performed on the TiO_x and TNO films, and the respective titanium 2p and oxygen 1s orbital peaks are illustrated in figures 3(*a*) and (*b*). The components (Ti^{2+} and Ti^{3+} in Ti 2p, oxygen deficiency in O 1s) related to signals arising from oxygen-deficient sites are more pronounced in the TNO film. Such a phenomenon was observed in an earlier publication [16], which is interpreted to occur from the Nb^{5+} ions substituting Ti^{4+} ions, thereby creating adjacent oxygen vacancies.

The valence band offsets with respect to the Fermi level were also measured by XPS, illustrated in figure 4. It is noteworthy that a larger concentration of midgap defects exist in the TNO film, which are anticipated to be related to the presence of Nb^{5+} ions. A former report on Nb-doped titanium oxide indicated the formation of midgap electronic states delocalized over the Ti t_{2g} orbitals and the Nb t_{2g} orbitals [12]. First-principles calculations indicated that such electronic levels would lie at approximately 2 eV above the valence band edge, which matches quite well with the peak in our experimental data.

The optical bandgaps for the TiO_x and TNO films were also measured by SE, as shown in figure 5. The bandgap

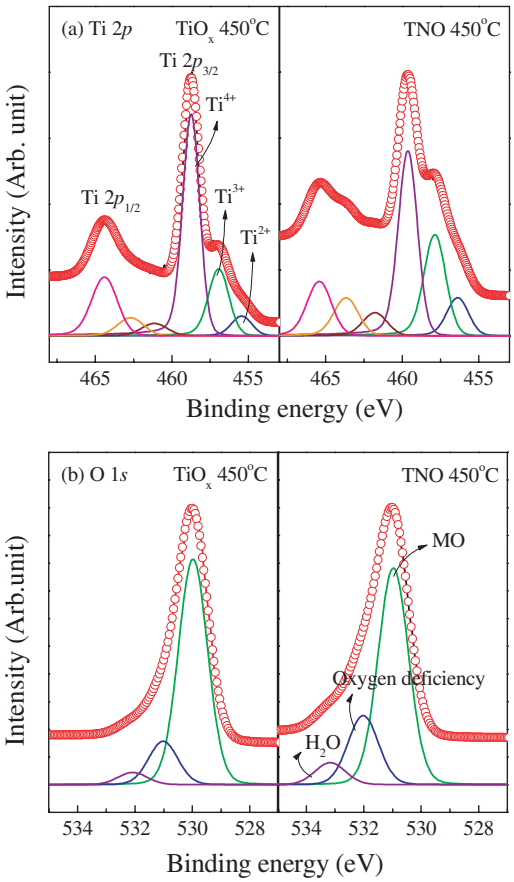

Figure 3. XPS peaks of (*a*) the titanium 2p orbitals from TiO_x and TNO film, and (*b*) the oxygen 1s orbitals from TiO_x and TNO film annealed at 450 °C. The main peaks are delineated in red, which are deconvoluted into sub-peaks.

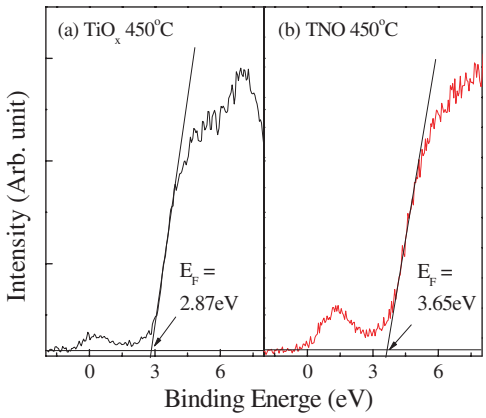

Figure 4. Valence band offsets measured by XPS analyses for the (*a*) TiO_x and (*b*) TNO films annealed at 450 °C. A peak associated with sub-gap defects appears in the spectrum taken from the TNO film.

values are approximately 3.69 eV for TiO_x, and 3.79 eV for TNO. Such a difference may have resulted from the different microstructure of the films, and also from the incorporation of niobium oxide, which is in general known to have a larger bandgap than titanium oxide. Although the values deviate from our results, rutile is known to have a bandgap of approximately 3.0 eV, and anatase is reported to have a slightly larger bandgap

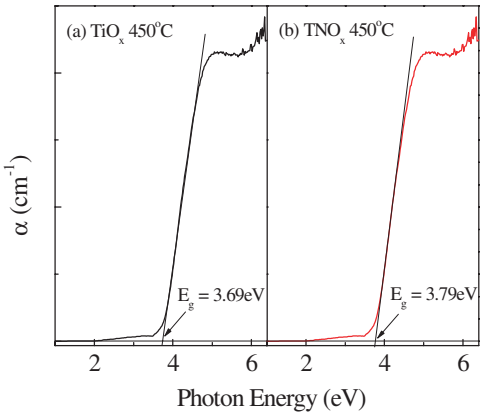

Figure 5. Absorption coefficient measured by SE for the (*a*) TiO_x and (*b*) film annealed at 450 °C. The TNO film exhibits a slightly larger optical bandgap.

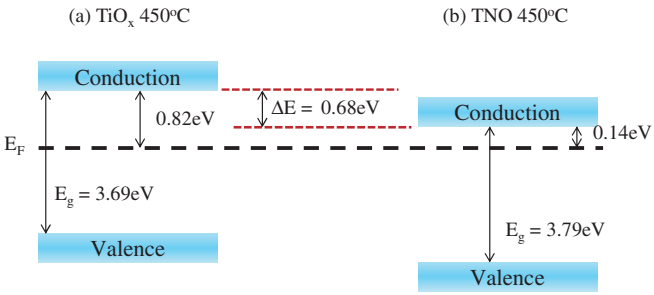

Figure 6. Schematic diagram of the relative position of the bandgaps between the (*a*) TiO_x and (*b*) TNO films annealed at 450 °C.

of 3.2 eV [13]. On the other hand, reports indicate that pure crystalline niobium oxide has a bandgap of 3.40 eV [14], and a larger value of 3.45 eV occurs when in an amorphous phase [15].

The above analyses such as optical bandgap and valence band edge are summarized as a relative position of Fermi level in figure 6. The Fermi level is closer to the conduction band minimum (E_C) in the TNO film, which is consistent with the fact that oxygen vacancies result in the generation of free carriers.

The electrical properties of the TFT devices are plotted in figure 7. Figures 7(*a*) and (*b*) represent the transfer characteristics of the TiO_x and TNO devices, respectively, showing the relationship between the gate voltage (V_g) and drain current (I_d). Figures 7(*c*) and (*d*) consist of the respective output curves, showing the relationship between the drain current and the drain voltage ($V_D = 10$ V).

The parameters such as field-effect mobility (μ_{fe}), threshold voltage (V_{th}) and subthreshold swing (S.S.) are summarized in table 1. The higher field effect mobility of the TNO device is attributed to the higher concentration of free carriers, and the formation of high conductivity paths by the presence of Nb^{5+} ions, as reported in a former article [16].

The device stability was evaluated with respect to positive and negative bias stress. A gate voltage of −20 V was applied in the case of negative bias stress, and +20 V for positive bias stress. The total stress time was 1 h for each device, and transfer curves were collected at 0 s, 100 , 1000 s and 3600 s of stress.

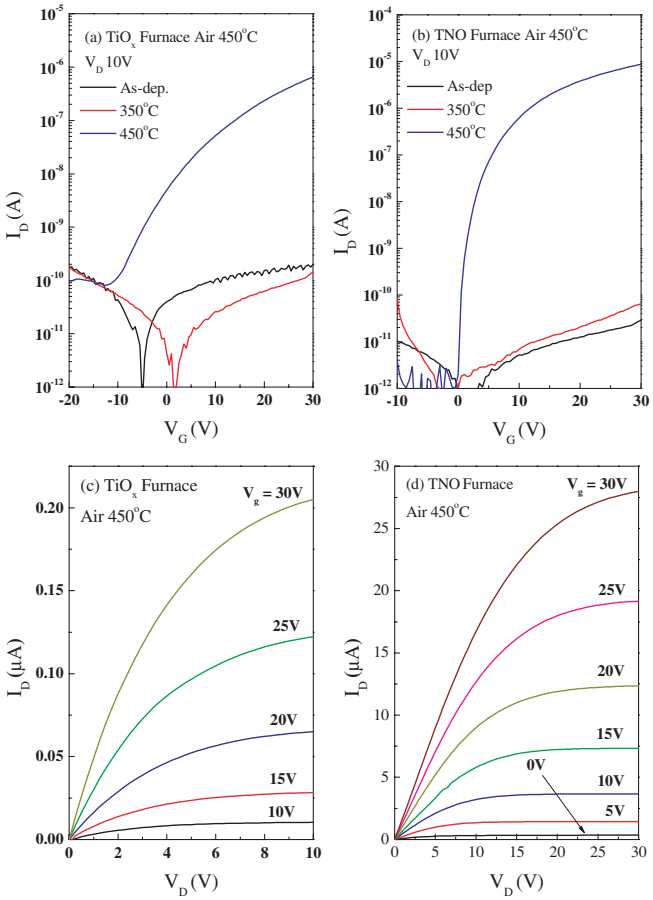

Figure 7. Transfer characteristics of the (*a*) TiO_x and (*b*) TNO devices. Output characteristics of the (*c*) TiO_x and (*d*) TNO devices.

Table 1. Electrical parameters for the devices using TiO_x and TNO films annealed at 450 °C.

	TiO_x (@450 °C)	TNO (@450 °C)
V_{th}	2.25 V	3.1 V
μ_{sat}	0.01 $cm^2\ V^{-1}\ s^{-1}$	0.13 $cm^2\ V^{-1}\ s^{-1}$
S.S.	4.96 V/dec.	0.5 V/dec.

The shifts in V_{th} (ΔV_{th}) are summarized in figure 8, and the ΔV_{th} values are listed in table 2.

In oxide semiconductor devices, positive shifts in V_{th} upon positive bias stress are often interpreted in terms of electron carrier trapping near the interface between the semiconductor and gate insulator [17, 18]. On the other hand, negative bias stress is usually explained to result from the trapping of positive hole carriers at the semiconductor-gate insulator interface. However, in n-type semiconductors such as In–Ga–Zn–O, hole trapping only occurs when a substantial amount of holes are present, which usually takes place when the devices are illuminated with visible light [19, 20]. An alternative explanation for the negative shift in V_{th} is based on the generation of excess electrons, which accumulate to the back surface of the semiconductor layer upon negative bias stress, while photo-generated holes remain localized near ionized oxygen vacancies and do not move [21].

The above XPS analyses indicate that defects related to oxygen vacancies are more abundant in TNO. In general, such

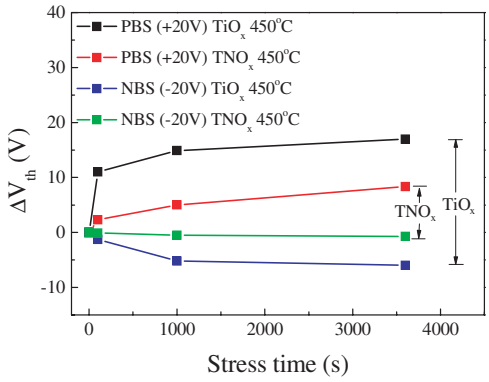

Figure 8. Evolution of the threshold voltage in the TiO_x and TNO devices with respect to bias stress time.

defects may be anticipated to act as carrier trap centres, which eventually result in faster degradation of devices upon bias stress experiments. However, the TiO_x and TNO devices presented in this work exhibit behaviours that cannot be explained in terms of oxygen vacancy sites, since the TNO device is more stable under both negative and positive bias stress. A plausible explanation for such counter intuitive results involves the presence of grain boundaries in TiO_x. Grain boundaries are well known to act as electron traps or scattering centres in polysilicon TFTs [22–24], and thus a similar influence may be found in TiO_x. While the grain boundaries act as scattering centres thus resulting in lower field-effect mobility in TiO_x devices compared to TNO devices, these defects act as charge traps, which induce more severe positive shifts in V_{th} upon positive bias stress. In the case of negative bias stress, the mechanism inducing large negative shifts in V_{th} in the TiO_x device is somewhat more complicated. It could either involve the trapping of holes, or the release of excess free electrons that were already trapped at the grain boundaries. Since the experiments were carried out in the dark, and TiO_x is an n-type semiconductor, the latter explanation is more reasonable. Although larger off current levels in the TiO_x device compared to the TNO device in figures 7(*a*) and (*b*) may lead us to suspect that holes are present in the semiconductor, such a fact is not experimentally substantiated at this point.

4. Conclusion

To summarize this work, the effect of niobium (Nb) doping on the performance and stability of TiO_x-based TFTs was studied. Sputtered TiO_x was initially amorphous and crystallized to anatase at an annealing temperature of 450 °C. On the other hand, Nb-doped TiO_x stays amorphous. TFT devices that use Nb-doped TiO_x as the active layer exhibited higher field-effect mobility and better stability upon negative and positive bias stress compared to pure TiO_x devices. Although XPS analyses indicated that TNO films have larger concentrations of oxygen vacancies and related defects, the effect of grain boundaries in crystalline TiO_x are believed to act as the major carrier traps, which then induce larger shifts in threshold voltage (V_{th}) upon both positive and negative bias stress.

Table 2. Evolution of the threshold voltage in the TiO_x and TNO devices with respect to bias stress time.

	ΔV_{th} (Threshold voltage instability)			
	Positive bias stress ($V_{GS} = 20$ V)		Negative bias stress ($V_{GS} = -20$ V)	
Stress Time (s)	TiO_x 450 °C	TNO 450 °C	TiO_x 450 °C	TNO 450 °C
0	0 V	0 V	0 V	0 V
100	11 V	2.33 V	−1.3 V	−0.1 V
1000	14.9 V	5.01 V	−5.2 V	−0.47 V
3600	17 V	8.37 V	−6 V	−0.7 V

Acknowledgments

This work was partially supported by 'the IT R&D program of MKE/KEIT (Grant No 10041416, the core technology development of light and space adaptable new mode display for energy saving on 7 inch and 2 W)' and 'the MKE/CITRC support program (NIPA-2012-H0301-12–4013) supervised by the NIPA'.

References

[1] Nomura K, Ohta H, Takagi A, Kamiya T, Hirano M and Hosono H 2004 *Nature* **432** 488
[2] Kamiya T and Hosono H 2010 *NPG Asia Mater.* **2** 15
[3] Furubayashi Y, Hitosugi T, Yamamoto Y, Inaba K, Kinoda G, Hirose Y, Shimada T and Hasegawa T 2005 *Appl. Phys. Lett.* **86** 252101
[4] Hoang N L H, Yamada N, Hitosugi T, Kasai J, Nakao S, Shimada T and Hasegawa T 2008 *Appl. Phys. Express* **1** 115001
[5] Yamada N, Hitosugi T, Kasai j, Hoang N L H, Nakao S, Hirose Y, Shimada T and Hasegawa T 2010 *Thin Solid Films* **518** 3101
[6] Mardare D and Hones P 1999 *Mater. Sci. Eng.* B **68** 42
[7] Gao Y 1999 *Thin Solid Films* **346** 73
[8] Matsushima S, Teraoka Y, Miura N and Yamazoe N 1988 *Japan. J. Appl. Phys.* **27** 1798
[9] Tang H, Prasad K, Sanjines R, Schmid P E and Lévi F 1994 *J. Appl. Phys.* **75** 2042
[10] Zhang Y, Ma X, Chen O and Yang D 2009 *J Alloys Compounds.* **480** 938
[11] Park J, Ok K-C, Ahn B D, Lee J H, Park J-W, Chung K-B and Park J-S 2011 *Appl. Phys. Lett.* **99** 142104
[12] Umebayashi T, Yamaki T, Sumita T, Yamamoto S, Tanaka S and Asai K 2003 *Nucl. Instrum. Methods* B **206** 264
[13] DeSario P A, Graham M E, Gelfand R M and Grav K A 2011 *Thin Solid Films* **519** 3562
[14] Kim J W, Augustyn V and Dunn B 2012 *Adv. Energy Mater.* **2** 141
[15] Yoshimura K, Miki T, Iwama S and Tanemura S 1996 *Thin Solid Films* **281–282** 235
[16] Ok K-C, Park J, Lee J H, Ahn B D, Lee J H, Chung K-B and Park J-S 2012 *Appl. Phys. Lett.* **100** 142103
[17] Suresh A and Muth J F 2008 *Appl. Phys. Lett.* **92** 033502
[18] Lee J-M, Cho I-T, Lee J-H and Kwon H-I 2008 *Appl. Phys. Lett.* **93** 093504
[19] Shin J-H, Lee J-S, Hwang C-S, Park S-H K, Cheong W-S, Ryu M, Byun C-W, Lee J-I and Chu H Y 2009 *ETRI J.* **31** 62
[20] Oh H, Yoon S-M, Ryu M K, Hwang C-S, Yang S and Park S-H K 2010 *Appl. Phys. Lett.* **97** 183502
[21] Ghaffarzadeh K, Nathan A, Robertson J, Kim S, Jeon S, Kim C, Chung U-I and Lee J-H 2010 *Appl. Phys. Lett.* **97** 113504
[22] Dimitriadis C A 1993 *J. Appl. Phys.* **73** 4086
[23] Maeda S, Maegawa S, Ipposhi T, Nishimura H, Ichiki T, Mitsuhashi J, Ashida M, Muragishi T, Inoue Y and Nishimura T 1994 *J. Appl. Phys.* **76** 8160
[24] Chen C-Y, Lee J-W, Wang S-D, Shieh M-S, Lee P-H, Chen W-C, Lin H-Y, Yeh K-L and Lei T-F 2006 *IEEE Trans. Electron Devices* **53** 2993